Sensors and Materials, Vol. 36, No. 2 (2024) 373–392
MYU Tokyo

S & M 3525

Monitoring Scheme of Liquified Natural Gas External Tank Using Air–Space–Land Integration Multisource Remote Sensing

Ming Guo,[1,2] Xingyu Tang,[1] Youshan Zhao,[3,4*] Yang Liu,[3,4]
Zhaorui Chen,[1,5] Li Zhu,[1] and Kecai Guo[6]

[1]School of Geomatics and Urban Spatial Informatics, Beijing University of Civil Engineering and Architecture, Beijing 102616, China
[2]Key Laboratory of Modern Urban Surveying and Mapping, National Administration of Surveying, Beijing 100044, China
[3]China Academy of Building Research, Beijing 100013, China
[4]CABR Testing Center Co., Ltd., Beijing 100013, China
[5]Lingnan University, Hong Kong 999077, China
[6]Beijing Shen Xin Da Cheng Technology Co. Ltd, Beijing 102444, China

(Received July 31, 2023; accepted October 25, 2023)

Keywords: LiDAR technology, UAV photogrammetry, InSAR technology, crack identification, program design

Liquefied natural gas (LNG) storage tanks are an essential infrastructure for national energy security, and the monitoring of their integrity is the basis for ensuring the regular operation of storage tanks. Existing monitoring methods do not reflect changes in storage tanks well because most monitoring methods are based on a technical approach that allows only one type of monitoring data to be obtained, which does not give comprehensive monitoring results. In this study, we incorporate control measurements, light detection and ranging (LiDAR), unmanned aerial vehicle (UAV) photogrammetry, thermal infrared camera monitoring, interferometric synthetic aperture radar (InSAR), and other techniques. An integrated air–space–land multisource remote sensing monitoring scheme is proposed, and the scheme's feasibility is verified through actual measurements, providing strong support for subsequent, efficient, and all-around monitoring.

1. Introduction

Liquefied natural gas (LNG) storage tanks are an essential infrastructure for national energy security.(1) With the rapid development of China's economy, the trend in LNG storage tanks is to expand the scale of production, large capacity, and higher demands on individual parameters.(2) As the size of the storage tanks increases, their potential risks also increase, and the chances of leakage and explosion accidents likewise gradually increase. Furthermore, LNG storage tanks can be overly deformed during the use of the tank wall for various reasons, resulting in its inability to play a protective role. For example, the wall of the tank may be thinned by corrosion, the ground may settle, and the liquid level inside the tank may rise and fall.(3) In addition, when

*Corresponding author: e-mail: yshzhao@163.com
https://doi.org/10.18494/SAM4603

ISSN 0914-4935

the external pressure of the tank is greater than the critical load of the tank wall, the tank body will produce instability, which may lead to failure.(4) High interity of the LNG external tank means that the LNG tank system will provide reliable service with structural integrity and functional integrity throughout its life cycle, provided that the medium inside the tank is in a stable operating condition. At the same time, there is no negative impact on the safety of the operator, the public in the vicinity, and the surrounding environment.(4,5) Therefore, monitoring the LNG external tanks is essential to ensure their safe operation. However, the existing related studies only focus on monitoring certain situations, such as land subsidence monitoring using interferometric synthetic aperture radar (InSAR) technology, analysis of force deformation using light detection and ranging (LiDAR) measurement data, and temperature change detection using an infrared thermal imaging camera. There is only one type of monitoring object, and the results of monitoring only settlement or deformation are not comprehensive enough to provide a strong basis for the overall safety maintenance of LNG tanks.

To solve the above problems, we will design a monitoring program to monitor the integrity of LNG external tanks through a methodology that incorporates station-based airborne LiDAR, unmanned aerial vehicle (UAV) scanning, thermal infrared detection, and InSAR monitoring of settling to realize the monitoring of the integrity of the external tank of an LNG storage tank with the integration of air–space–land and multitechnology fusion, to ensure the rationality and feasibility of the implementation of monitoring technology, and to guide the orderly development and successful completion of the integrity monitoring of an LNG storage tank.

2. Monitoring Area Overview and Methodology

2.1 Monitoring area overview

The LNG storage tanks are located in the harbor area along the coast and is of a mixed tide type where irregular daily tides dominate. In the high tide season, there is a full-day tide for 22 days per month on average. In the low tide season, there is a half-day tide for 8 days per month on average. The maximum tide level is 5.55 m and the minimum tide level is 0.03 m. The maximum tide difference is 5.36 m, the minimum tide difference is 0.17 m, and the average tide difference is 2.55 m. Cyclic changes in tides can cause the expansion and contraction of LNG storage tank structures, which can lead to cracks in the tanks, resulting in situations with ecological damage and threats to the safety of construction workers.

The main construction work of the LNG project includes hydraulic wharf buildings, shore protection, harbor pond dredging, inflow submerged dike, intake and discharge port hydraulic buildings, ship-to-shore communication, and auxiliary berthing systems (Fig. 1).

The main target of this LNG tank monitoring is the integrity of the external tank. The tank structure is an axisymmetric body comprising a cylinder topped with a dome. The outermost radius is about 42 meters, and the total height is about 60 meters (Fig. 2).

Fig. 1. (Color online) Monitoring area map.

Fig. 2. (Color online) The target LNG storage tank of the study.

2.2 Monitoring methods

The research related to the safety monitoring technology of large LNG storage tanks includes the real-time monitoring of temperature, strain, sedimentation, displacement, and deformation of large storage tanks.[2,3,5] Therefore, we monitored the integrity of the LNG external tank through air–space–land integration multisource remote sensing monitoring technology, integrating total station control measurement, LiDAR measurement, UAV photogrammetry, infrared thermal camera measurement identification, and InSAR settlement monitoring (Fig. 3).

The main research includes: control measurements are made using two instruments, the total station and the rtk (which acquires the Beidou signal), to obtain the control point coordinates, on the basis of which the point cloud data of the external tank with correct coordinates are acquired

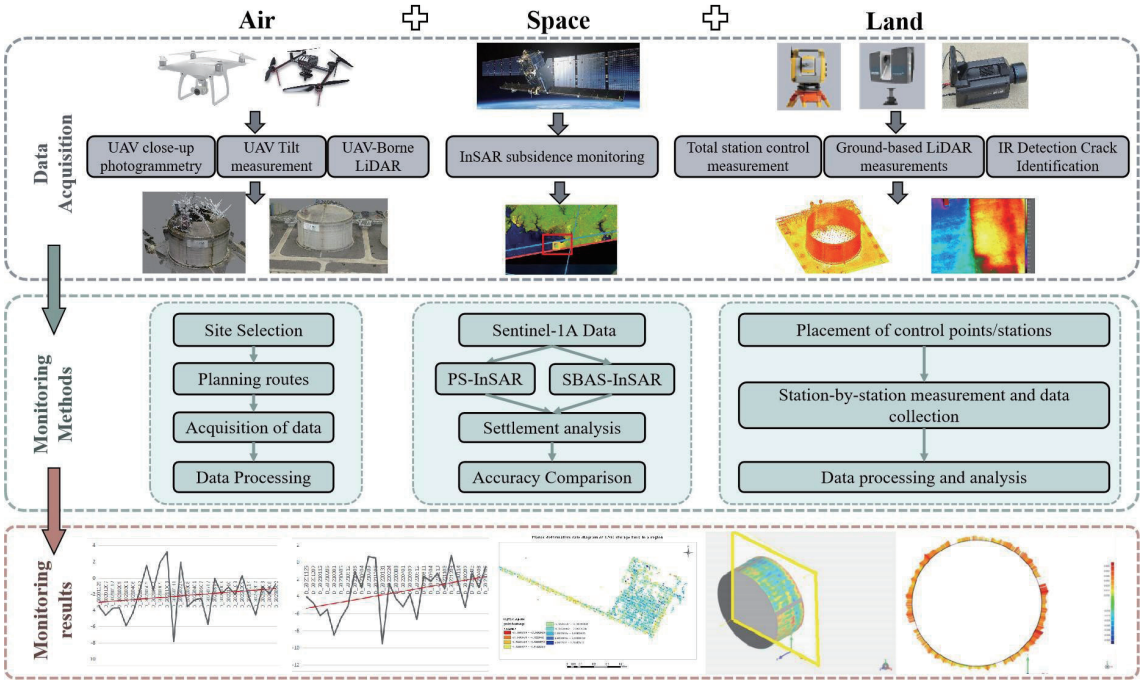

Fig. 3. (Color online) Monitoring methods.

by station-borne LiDAR and UAV airborne LiDAR. The images obtained by UAV photogrammetry are converted into point clouds, then registration of the generated point cloud with the point cloud acquired by LIDAR to analyze the deformation of the storage tanks. Thermal infrared detection is used to obtain temperature variations in the external tank and to identify where cracks exist. Afterwards, a neural network is used to extract the cracks, which are then matched with the point cloud data. Finally, the land subsidence at the location of the LNG storage tank is determined by InSAR technology.

2.3 Monitoring instrument

1. Total station instrument
   Total stations for control surveys are characterized by high accuracy, reliability, and durability for a wide range of surveying tasks. The specific parameters are shown in Table 1.
2. UAV equipment
   The UAV equipment used for this measurement is equipped with a 20 megapixel camera having an image element size of 2.4 μm and a focal length of 8.8 mm. The angle that the camera can be adjusted by the pan-tilt is −90°–30°, and the shooting range is wide. The specific parameters are shown in Table 2.
3. LiDAR equipment
   A Faro scanner was used for the ground-based LiDAR monitoring. Its main performance parameters are shown in Table 3.

Table 1
Main performance parameters of total stations.

Performance indicators	Performance parameters
Angular accuracy	0.5 s
Accuracy of ranging	0.6 mm + 1 ppm
Nonangular ranging	1000 m
Angle measurement method	Absolute coding, continuous, quadruple angle detection
ATR working distance	Maximum: 1000 m; general: 700 m
ATR precision	Basic accuracy: 1 mm

Table 2
Main performance parameters of UAV.

Performance indicators	Performance parameters
Maximum ascent speed	Movement mode: 6 m/s
Maximum descent speed	Movement mode: 4 m/s
Maximum horizontal flight speed	Movement mode: 72 km/h
Maximum tiltable angle	Movement mode: 42°
Maximum takeoff altitude	6000 m
Maximum flight time	28 min
Ambient temperature	0–40 ℃

Table 3
Main performance parameters of Faro scanner.

Performance indicators	Performance parameters
Laser emission frequency	100 million points/s
Measurement range	150 m
Zero bias gyroscope	≤0.001 °/h
Scanning angle resolution	0.0088°
Angular velocity measurement range	±400 °/s
Scanning angle	300° Longitudinal/360° Horizontal
Environmental adaptability	Temperature: −10–50 ℃; Humidity: 0–95%

In our study, the airborne LiDAR used a UAV from Pegasus with a Livox LiDAR scanner. The parameters of the specific instrument are shown in Table 4.

4. Infrared camera
   An infrared camera from FLIR was used for this monitoring. The camera uses an advanced 640 × 512 read-out integrated circuit in conjunction with a mercury telluride detector. The camera covers the middle-infrared band from 1.5–5.5 μm and generates 14-bit thermal image data. The specific parameters of the thermal imaging camera are shown in Table 5.

3. Multisource Remote Sensing Monitoring Core Technology

3.1 Total station control measurement

3D laser scanning technology can obtain the 3D spatial point cloud data of LNG storage tanks. To convert the relative coordinate system coordinates of the point cloud data to absolute or

Table 4
Main performance parameters of Livox LiDAR.

Drone		Lidar	
Performance indicators	Performance parameters	Performance indicators	Performance parameters
Weight of empty machine	2.6 kg	Laser wavelength	905 nm
Navigation satellite	Bei Dou, GPS	Field of view	14.5° × 16.2°
Maximum load capacity	750 g	Distance accuracy	2 cm
Maximum speed of aircraft	20 m/s	Angle accuracy	< 0.03º
Longest voyage	50 km	Beam divergence	0.12° (Vertical) × 0.02° (Level)
Maximum flight time	74 min	Field of view coverage	99.8% @0.1 s²

Table 5
Main parameters of the thermal imaging camera.

Performance indicators	Performance parameters
Detector type	Focal Plane Array, FPA
Infrared image resolution	640 × 512
Spectral range	1.5 – 5.5 μm
Temperature measurement accuracy	±1 ℃ (1.8 ℉) or ±1%
Detector spacing	15 μm
Maximum image frequency (full frame)	146 Hz
Integration time range	80 ns–20000 μs
External power supply	24 V DC, 48/35 W PC

local coordinate system coordinates, it is necessary to perform control measurements using a total station and RTK receiving Beidou signals to obtain the coordinates of selected control points in an absolute coordinate system so as to perform coordinate conversion.(6)

3.1.1 Layout of control points and reflector plates

From among the existing control points at the LNG tank site, three points, namely, G17, G18, and G19, near the target tanks were selected as control points for control measurements after the site survey. Afterwards, reflector plates were attached on the tank wall at positions where the control point is visible, as shown in Fig. 4.

Reflector plates should be placed to meet the following requirements: there is no obstruction between them and the control points; two neighboring reflector plates should not be on one line so that one should be placed high and the other low to facilitate the calculation of coordinate conversion. Owing to the large height of the tank and safety issues, it is inconvenient to place the reflective sheet at locations higher than 2 meters. Therefore, a total of 13 points are laid out at the bottom of the tank. The specific locations of the reflector plates are shown in Fig. 5.

3.1.2 Control points and attaching of reflective sheet

The role of control measurement is to limit the propagation and accumulation of measurement errors, to ensure the necessary measurement accuracy, so that the measurement work carried out in subdistricts can be connected as a whole and the overall design of the measurement program

(a) (b)

Fig. 4. (Color online) Attaching reflective sheet. (a) Site of attaching reflective sheet. (b) No. 12 reflector location.

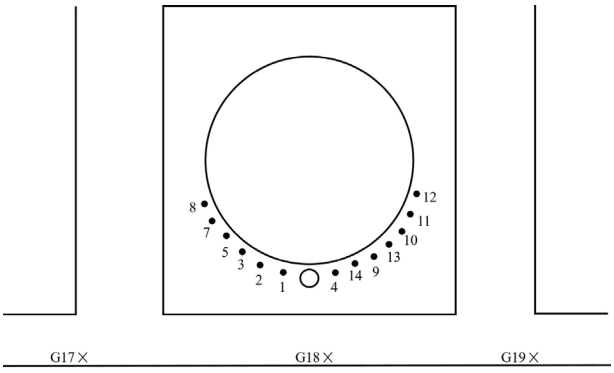

Fig. 5. Reflector placement locations.

can be obtained in a coordinate system on the basis of the results.[7] Control measurement is divided into plane control survey and elevation control survey. The purpose of plane control survey is to determine the plane position of the control point (X, Y), and the purpose of elevation control survey is to determine the elevation of the control point (H).

We observe and measure the established control points with measuring equipment to obtain their accurate spatial coordinates or shape and dimension information. The observation method can be selected in accordance with specific measurement needs. In this study, we used a total station to measure angles and distances, and its elevation can be obtained from the coordinates of ground points collected by RTK with the assumed altitude measurement of the total station. The obtained measurement data of the control points are processed and evaluated, such as coordinate adjustment and data accuracy evaluation. This improves the accuracy of the control

points and reduces the transmission of survey errors. The collected coordinates provide the coordinate basis for subsequent measurements. The coordinates of some control points are shown in Table 6.

3.2 UAV photogrammetry technology

UAV photogrammetry is the use of image data acquired by aerial photography using drones. Information on the spatial location, shape, size, and surface texture of features is obtained through measurement, analysis, and processing by photogrammetry techniques. The flexibility and efficiency of UAVs make photogrammetry more convenient and accurate than traditional photogrammetry.[8]

3.2.1 Control points and reflective sheet laying

3.2.1.1 Close-up photogrammetry

Drones are equipped with cameras or sensors to take aerial photographs at a certain altitude and speed to collect image data. Aerial photography requires the consideration of parameters such as route design, flight height, and overlap to obtain high-quality image data. The acquired image data must be geometrically corrected, including camera pose correction and aberration correction.[9] Camera pose correction is the alignment of ground features in the image with the UAV pose and the elimination of the effects caused by the camera pose. Aberration correction corrects the aberrations of the camera lens so that the image has accurate geometric characteristics.[10,11] Through image processing techniques, feature extraction is performed on the corrected images to extract feature points such as boundaries, corner points, and textures of features. The commonly used feature extraction algorithms include Scale Invariant Feature Transform (SIFT) and Speeded-Up Robust Features (SURF).[12]

After that, it is necessary to match the feature points, that is, to correlate the feature points of the same feature in different images and establish the feature point correspondence. Lastly, the 3D coordinates of the acquired features are subjected to data processing, accuracy evaluation, alignment, and other operations to generate point cloud data, a digital elevation model (DEM), and other products for subsequent analysis and application.

Table 6
Coordinates of control points.

Point number	*X*	*Y*	*Z*
G17	**216.921	**2937.883	7.989
G18	**298.250	**2900.929	7.986
G19	**288.275	**2860.062	7.984
1	**320.573	**2922.634	8.860
2	**313.768	**2928.444	7.167
3	**308.476	**2933.157	8.265
4	**329.155	**2919.522	6.888
5	**305.329	**2939.219	7.444

3.2.1.2 Measurement solutions and data

First, with the target LNG storage tank as the center, the focus of the camera is kept unchanged, so that the UAV and the tank maintain a certain distance while pictures are being taken. Perform multi-height close-up photography from the top to the bottom of the tank, making sure that each photo is taken at the same distance from the tank and that there is a 70 to 80 percent overlap between the top and bottom adjacent photos. Then, we repeat the previous operation 360° around the tank so that the photos cover all surfaces of the target tank. We also ensure that the overlap between routes is around 60%. The specific flight path is shown in Fig. 6, and the blue shading shows where photographs were taken. Note that when drones are used for close-up photography operations, because of the effects of lighting, the aperture, shutter speed, ISO, and other parameters must be changed each time to ensure that the acquired images are uniform in color.

Finally, the collected image data are imported into computer software, registered, stitched together, and reconstructed in 3D to generate a 3D dense point cloud using the SfM algorithm, as shown in Fig. 7. Finally, a 3D model is generated. Since the close-up photogrammetry mainly yields images of the tank body, the quality of the generated top point cloud data is poor, and UAV oblique photography is needed to generate better top point cloud data.

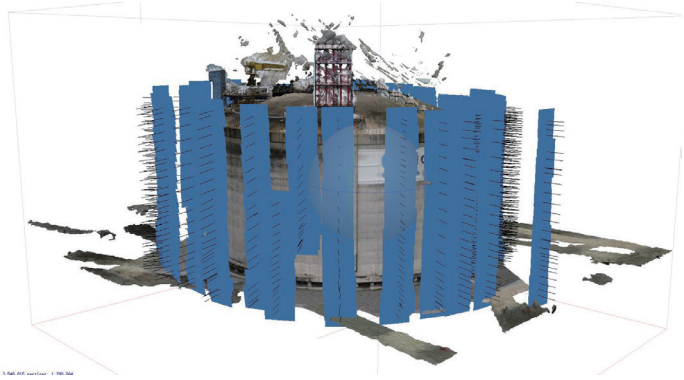

Fig. 6. (Color online) Close-up photogrammetric route.

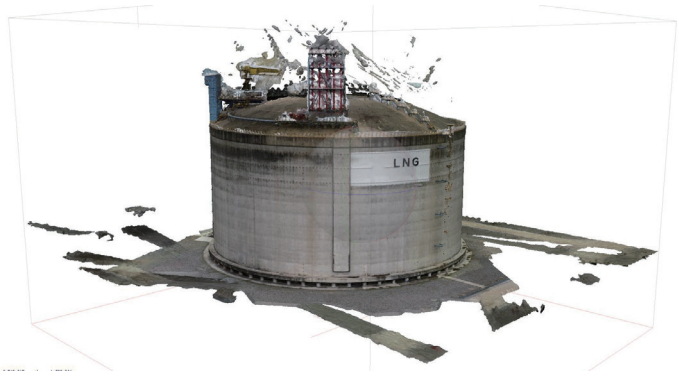

Fig. 7. (Color online) Point cloud data generated from close-up photogrammetry.

3.2.2 UAV oblique photography measurement

UAV oblique photography is a method of acquiring three-dimensional information of the ground surface through oblique photography technology. Compared with traditional aerial photography, oblique photography can obtain higher resolution, more directions, and more accurate 3D data.[13] The concept is to obtain image data from different angles and perspectives by mounting the camera on the drone at an angle and taking continuous shots along a set heading. By processing the image data, three-dimensional information about the ground surface can be obtained.

3.2.2.1 Oblique photogrammetry

Oblique photography equipment usually consists of multiple cameras or sensors mounted on the load platform of a UAV. These cameras or sensors are oriented towards the ground at a certain tilt angle and can cover a certain heading and longitudinal range at the same time. The drone flies in accordance with a preset course while the camera continuously captures images of the ground. During the flight, the drone maintains a certain tilt angle so that the images captured contain ground information from different angles and perspectives.

The image data taken with the oblique photography equipment can be used to obtain a high-resolution image of the ground. Owing to the tilt angle of the camera and continuous shooting, the image data have a better spatial sense and perspective, which can provide more detailed and realistic information on the terrain. The acquired tilt images require image processing. This includes correction of camera pose, aberration correction, and image stitching.[14] These processing operations ensure that the image data have accurate geometric features and consistency, providing the basis for subsequent data processing. The image data from oblique photography, combined with techniques such as photogrammetry and computer vision, can be used for data processing and analysis operations such as image matching, 3D reconstruction, point cloud generation, digital surface modeling, and digital elevation modeling to obtain 3D information of the features.

3.2.2.2 Measurement solutions and data

The first step is to plan the flight route of the UAV; the planning should take into account the actual situation of the survey area and the performance requirements of the equipment. Digital images of the area around the LNG target tanks, which is about 0.12 km^2, were taken by low-altitude photography from a UAV, and digital orthophoto maps at the 1:500 scale were produced. At the same time, using the image data and the method of aerial mapping, a 1:500 topographic map is supplemented for the 0.37 km^2 area around the LNG storage tank. This was followed by combining the full field topographic map data to synthesize a complete 1:500 scale topographic map of the area around the LNG storage tanks.

We take the target storage tank as the center and the area expanded 30 m outward as the measurement area. We set the heading height to 80 m, heading overlap to 80%, side overlap to

70%, and route spacing to 40 m. Oblique photography was performed above the tanks following a vertical and horizontal cross course, as shown in Fig. 8, with the blue shading showing where the photographs were taken.

Finally, the collected image data are imported into the relevant computer software. The processing flow is the same as that of close-up photogrammetry, and the generated data are shown in Fig. 9. Compared with close-up photography, oblique photography acquires images of the top, so the quality of the generated top-point cloud data is better.

3.3 Ground-based and unmanned airborne LiDAR data acquisition and fusion

The 3D laser measurement and acquisition equipment integrates a high-precision 3D scanner, control and storage module, HD panoramic camera, and other sensors, enabling it to quickly obtain high-quality 3D point clouds of the surrounding environment.[15] It is characterized by flexibility, speed, high precision, high resolution, safe and reliable data, and comprehensive information.[16]

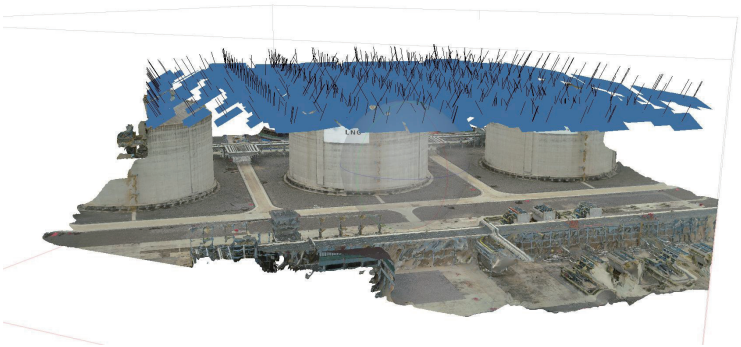

Fig. 8. (Color online) Inclined photogrammetry route.

Fig. 9. (Color online) Oblique photography to generate point cloud data.

3.3.1 Ground-based LiDAR measurements

The monitoring is carried out by erecting stations and gradually advancing the operation. The whole system consists primarily of a ground-based 3D laser scanner and postprocessing software. The scanning method is noncontact scanning to obtain the 3D point cloud data of the LNG external tank. The collected point cloud data are finally processed by the postprocessing software to generate the point cloud model of the LNG storage tank. Project implementation steps include external data collection, internal data processing, and collation of results of the three main elements.[6,15] The foreign industry data collection includes on-site scanning and digital photography. Internal data processing includes tasks such as scanning point cloud stitching and denoising and point cloud registration.

When data acquisition is based on a 3D laser scanner, the collected point cloud data are susceptible to factors such as the environment and scanning system, causing redundant data, such as noisy data points that do not belong to the scanned object itself, to be produced. Therefore, the point cloud data must be denoised and smoothed to improve the accuracy of the final results. Subsequently, all the point cloud data will be imported into the relevant software for splicing and registration, and the error should be controlled at about 4 mm. The stitched point cloud data shown in Fig. 10 are used to generate a point cloud model for subsequent data support of monitoring and analysis.

3.3.2 UAV airborne LiDAR measurements

The UAV airborne LiDAR consists of Pegasus UAV equipment equipped with Livox LiDAR scanning equipment. This includes an inertial guidance system consisting of inertial guidance and IMU for determining precise flight transient pose parameters, namely, heading angle, side angle, and inclination angle, GPS to accurately determine the location information of the UAV, and a LiDAR scanner to acquire point cloud data of all target objects under the flight path.[15,16] The pose information was determined by the combined inertial guidance system, the GPS

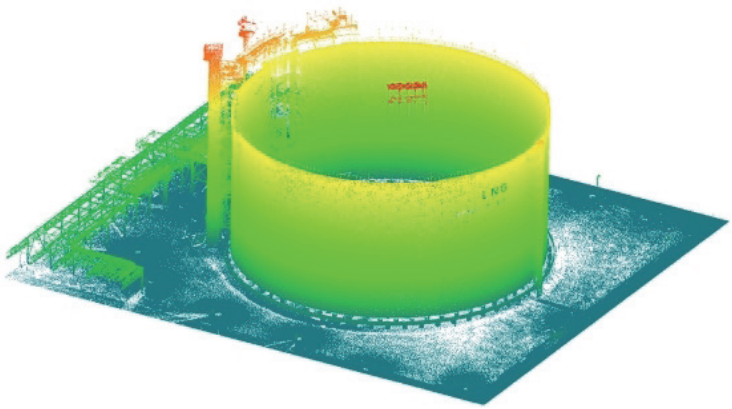

Fig. 10. (Color online) Point cloud data acquired by ground-based LiDAR.

position information, and the control point coordinate information obtained by the control survey. The point cloud data are processed by tasks such as stitching, denoising, and coordinate conversion to finally obtain a more accurate point cloud model.

The first step is to explore and survey the site, determine the flight area, and plan the flight path. As shown in Fig. 11, the purple part is the flight range set for this scan, and it covers the LNG storage tanks as well as the flat surface in their vicinity. The total area is approximately 0.096 km^2. The yellow lines indicate the planned flight path. The route spacing is about 30 m. The flight speed is 14 m/s, the flight height is 110 m, and the side overlap is greater than 70%.

After the measurement is completed, the acquired data is exported from the LiDAR scanner to computer software. We perform data preprocessing, including data splicing, denoising, and smoothing, to obtain the complete point cloud data and assign a color to each flight strip (Fig. 12). The coordinates of the point cloud data are converted to the world coordinate system by performing coordinate transformation from the absolute coordinates obtained by the control measurement.

3.3.3 Data fusion and processing

The point cloud data acquired by ground-based LiDAR and airborne LiDAR are converted to a unified world coordinate system with the same control points to ensure the accuracy of

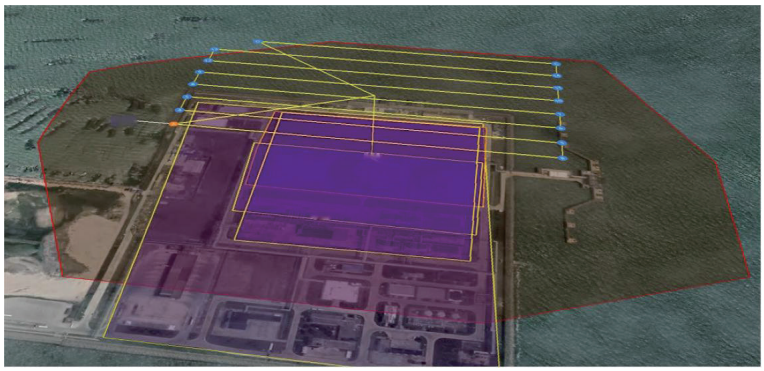

Fig. 11. (Color online) UAV airborne LiDAR routes.

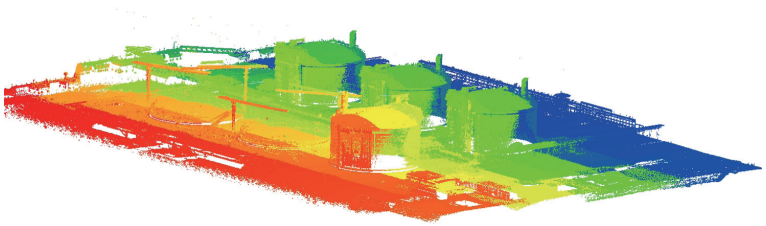

Fig. 12. (Color online) UAV airborne LiDAR acquisition of point cloud data.

subsequent point cloud fusion. The two sets of data are registered by the iterative closest point method to achieve fusion.[17] We obtain more completed and detailed point cloud data of the external surface of LNG storage tanks.

The fusion point cloud data is later cut, specifically by cutting in lines parallel to the ground in the direction of the tank perpendicular to the ground. The cut section is used to encapsulate and fit the standard column. The fitting method used is a random sampling algorithm: random sample consensus. The deformation of the tank surface was derived by analyzing the deviation between the fitted value and the measured value by both 3D comparison and 2D comparison of the data. The standard column was obtained by fitting a height of 36.596 m and a diameter of 83.510 m. A comparison with the measured values shows an overall average deviation of around 0.0169 m (see Fig. 13).

3.4 Infrared thermal imaging camera for external tank crack identification

Infrared thermal imaging nondestructive testing technology refers to technology to detect invisible infrared energy emitted by the object being tested by means of an infrared thermographic camera without damaging the performance of the object being tested and then to convert it into an electrical signal that can be measured.[18] The temperature distribution on the surface of the object being inspected can be seen on the infrared thermal image. On the basis of the surface temperature distribution, it is possible to determine whether there are discontinuous defects in the object being inspected.

3.4.1 Measurement methodology

The monitoring principle is that when fissures exist inside an LNG storage tank, they cause a local change in the thermal conductivity of the tank. Fissures impede the transfer of heat when subjected to external thermal excitation.[18] If the temperature inside the storage tank is not evenly distributed, this will eventually cause a change in surface temperature.

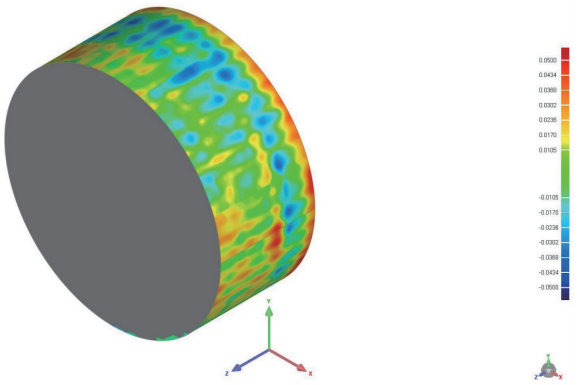

Fig. 13. (Color online) Difference between standard column fit and measured value.

The thermal infrared camera is used to scan for places where cracks may exist in the LNG external tanks. Because of the limited range of the camera and the large size of the LNG storage tanks, the surface temperature data are collected in the following ways: in the direction parallel to the horizontal plane, by taking pictures at 45° intervals starting from the center of the front of the tanks, and in the direction perpendicular to the horizontal plane, by taking pictures progressively from the bottom to the top of the tanks. The collected data are processed by the accompanying software in the computer to generate an image of the temperature distribution in the LNG storage tank [as shown in Fig. 14(a)]. This image is used to observe the temperature distribution of the monitoring target. Different temperature zones correspond to different colors. The brighter the color, the higher the temperature, and conversely, the darker the color, the lower the temperature. From the temperature distribution of the external tank, cracks are identified and extracted by a convolutional neural network, so as to determine the location of the cracks and to judge the size of the cracks, as shown in Fig. 14(b). In the bottom layer of the external tank, four cracks due to gravity and humid climate were extracted in the area of 640 × 512 pixels, and the comparison with the original image proved that the extraction results were highly accurate.

3.5 InSAR settlement monitoring

3.5.1 Data sources

3.5.1.1 Sentinel-1A

The Sentinel-1A satellite was launched by ESA in April 2014 from Kourou, Guyana, France. The orbital altitude is 693 km, and it carries a C-band synthetic aperture radar. It has a 12-day

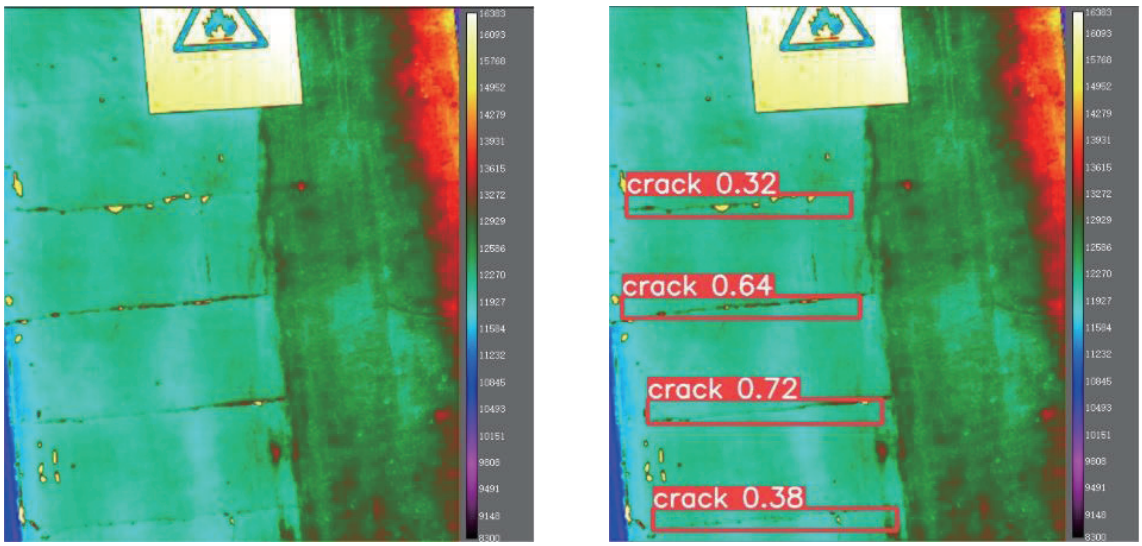

(a) (b)

Fig. 14. (Color online) Results of thermal imaging camera capture identification. (a) Temperature distribution image. (b) Identifying crack images.

revisit interval and a wide range of polarization options and operating modes. The Sentinel-1A satellite has four imaging modes: stripmap imaging, interference wide, ultrawide, and wave modes. The Earth observation mode is interference width.[19] The specific parameters are shown in Table 7.

3.5.1.2 DEM

The DEM is from the Shuttle Radar Topography Mission (SRTM), a joint effort between the German and Italian space agencies, the National Aeronautics and Space Administration, and the National Mapping Agency of the Department of Defense. SRTM topographic data can be divided by resolution into SRTM1 data at 30 m resolution and SRTM3 data at 90 m resolution.[20] Our monitoring uses 30 m resolution SRTM1 data (as shown in Fig. 15).

3.5.2 Monitoring methods

Persistent scatterer interferometric synthetic aperture radar (PS-InSAR) technology and small baseline subset interferometric synthetic aperture radar (SBAS-InSAR) technology were used in our monitoring. Thirty-one Sentinel-1 observation data from August 2020 through May 2023 were selected for the monitoring. The overall flow chart is shown in Fig. 16.

Table 7
Sentinel-1A satellite imaging mode parameters.

Pattern	Angle of incidence (/°)	Resolution (/m)	Width (/km)	Polarization mode
Stripmap imaging	20–45	5 × 5	80	fully polarized
Interference width	29–46	5 × 20	250	fully polarized
Ultrawide	19–47	20 × 40	400	fully polarized
Wave	22–35	5 × 5	20 × 20	HH,VV

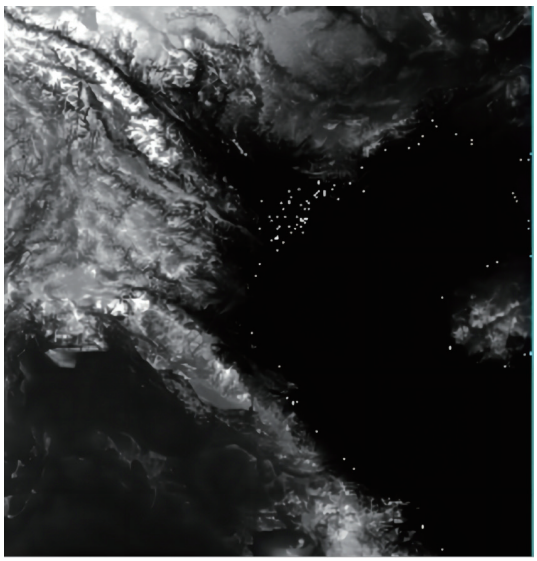

Fig. 15. DEM data.

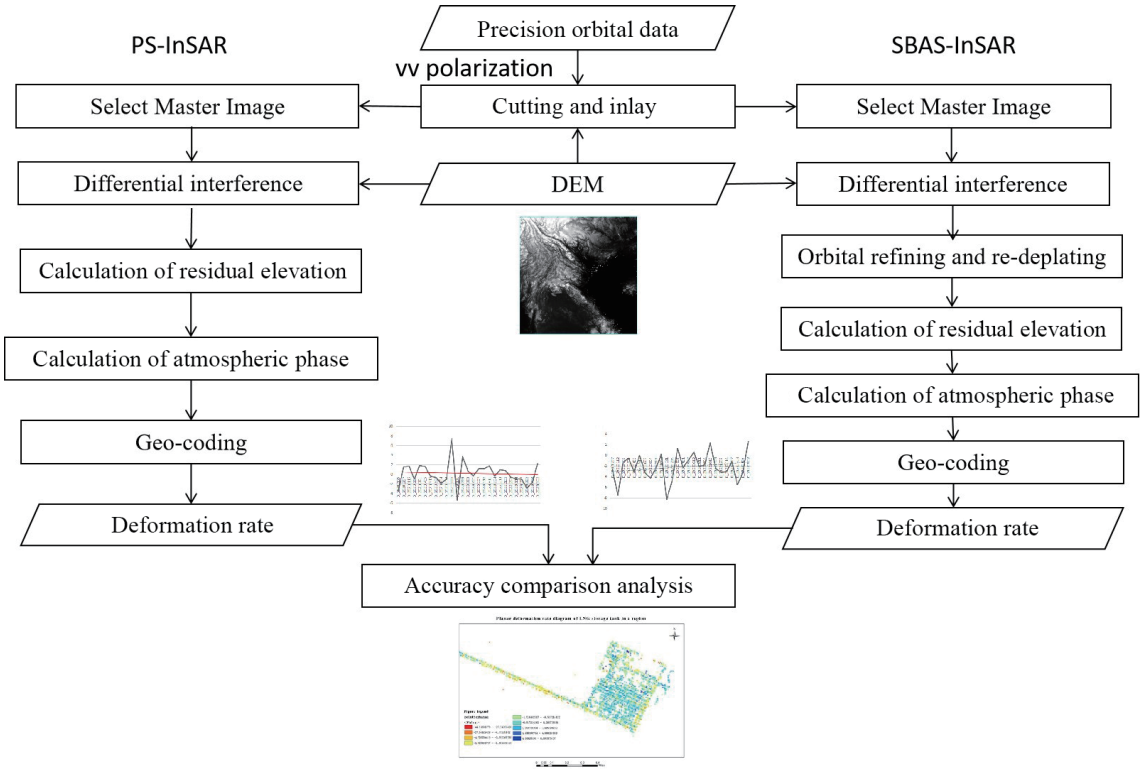

Fig. 16. (Color online) Flow chart of InSAR technology.

3.5.2.1 PS-InSAR

The PS-InSAR technique selects a master image from the SAR images of the same study area. Multiple temporal interferometric image pairs are obtained by registering all other images and sampling them into the master image. From these interferometric image pairs, persistent scatterers (PS points) with more stable radar scattering characteristics are selected and extracted.[21] Finally, the differential interferometric processing of the received echo phases is continued to analyze the spatial autocorrelation of the neighboring points.

3.5.2.2 SBAS-InSAR

The SBAS-InSAR technique is a time series analysis method for the study of low-resolution, large-scale deformations.[18] Firstly, a series of interferograms are generated by setting spatiotemporal baseline thresholds to combine the images freely, and the surface deformation information is solved by the least-squares method.[22] Time series analysis is then carried out by the singular value decomposition method of matrices to find the least squares solution of the smallest paradigm to remove the residual terrain and solve the time discontinuity problem. Finally, multiple short baseline sets of data are combined and inverted to obtain information on surface deformation and the average deformation rate over the observed time period.

3.5.3 Comparison and analysis of the accuracy of results

To determine the accuracy of the results, the deformation results of PS-InSAR and SBAS-InSAR techniques are compared (as shown in Fig. 17). Separate deformation rate maps are extracted for the two techniques. The difference between the two deformation rate results is compared to verify the accuracy of the results of the monitoring.

The InSAR sedimentation rate results were obtained and are shown in Fig. 18. The average annual sedimentation rate obtained by the PS-InSAR technique is in the range of −2.5–2 mm/year, and the cumulative sedimentation is in the range of −10.7932834625–5.483941555 mm/year. The annual average sedimentation rate obtained by SBAS-InSAR is in the range of −3.5–3mm/year, and the cumulative amount of sedimentation is in the range of −9.2934564625–6.356975264 mm/year. The settling rates determined by the two methods are approximately the same and the overall stability is favorable.

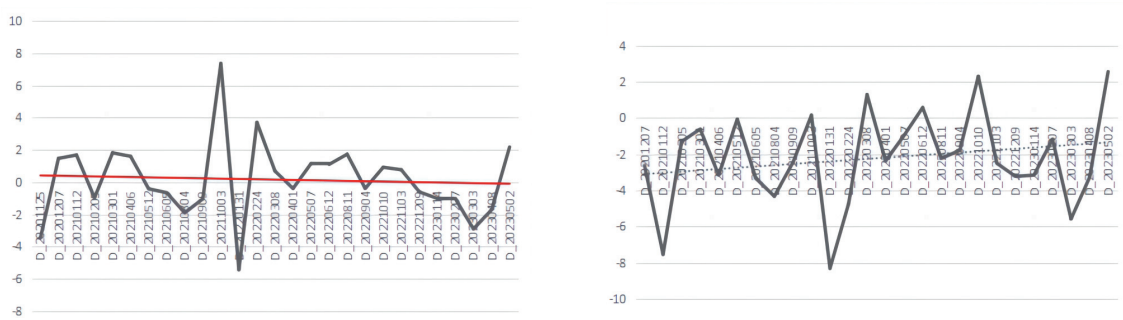

(a) (b)

Fig. 17. (Color online) PS-InSAR and SBAS-InSAR results. (a) Folded graph of the change in settlement at a PS point. (b) Folded graph of the change in settlement at a point of SBAS.

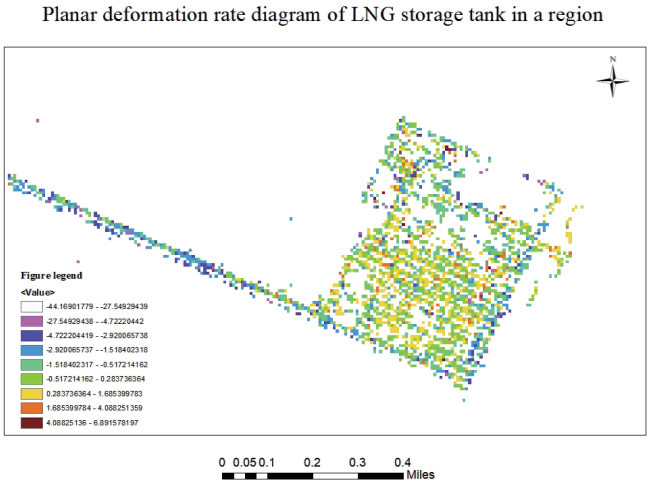

Fig. 18. (Color online) InSAR sedimentation rate results.

4. Conclusions

The analysis of LNG tank safety monitoring methods revealed some problems, such as the monitoring of only one research object by one technique, which leads to insufficient comprehensiveness and completeness of the obtained monitoring results. Focusing at the above problems, we designed a monitoring program of the integrity of LNG external tanks by integrating ground-based and unmanned airborne LiDAR, UAV photogrammetry, thermal infrared detection, and InSAR settlement techniques to realize the monitoring of the integrity of LNG external tanks by air–space–land integration and multitechnology fusion. After actual measurements, the average deviation of the tank as a whole was found to be around 0.0169 m, and the settlement rate in this area was between −3 and 2.5 mm/year. The results validate the feasibility of our solution of combining several technologies to compensate for the shortcomings of each technology. The multisource data obtained allow for an effective all-around analysis of the integrity of LNG storage tanks. This multisource data provides a robust monitoring methodology and data support for follow-up monitoring and also provides an effective and feasible monitoring solution for similar types of storage tanks.

Acknowledgments

This research was supported by the Research Fund of CABR Testing Center Company (20220126977130008), Research Fund of China Academy of Building Sciences Company (20220112330730019), National Key RD Program of China (2022YFF0904400, 2021YFF0602005-03), National Natural Science Foundation of China (41971350, 42171416), Teacher Support Program for Pyramid Talent Training Project of Beijing University of Civil Engineering and Architecture (JDJQ20200307), and Categorical Development Quota Project - Master's Degree Innovation Project (2023) (PG2023117).

References

1 S. Peng, D. Zhou, and B. Xie: Appl. Sci. **12** (2022) 23. https://doi.org/10.3390/app122311941
2 N. Sharari, B. Fatahi, A. Hokmabadi, and R. Xu: Bull. Earthquake Eng. **20** (2022) 7. https://doi.org/10.1007/s10518-022-01384-1
3 C. Wang and Y. Ju: Cryogenics **120** (2021) 103373. https://doi.org/10.1016/j.cryogenics.2021.103373
4 H. Yu, Y. Yi, A. Romagnoli, and W. Tan: Cold Reg. Sci. Technol. **194** (2021) 103438. https://doi.org/10.1016/j.coldregions.2021.103438
5 Z. Fu and T. Shan: Nafural Gas Ind. **32** (2012) 2. https://doi.org/10.3787/j.issn.1000-0976.2012.03.020
6 M. Guo, B. Yan, T. Zhou, Z. Chen, C. Zhang, and Y. Liu: J. Archit, Civil Eng. **37** (2020) 2. https://doi.org/10.19815/j.jace.2019.03061
7 Z. Yang, X. Guo, and X. Liu: J. Beijing Univ. Civil Eng. Archit. **36** (2020) 4.
8 M. Guo, M. Sun, D. Pan, G. Wang, Y. Zhou, B. Yan, and Z. Fu: Heritage Sci. **11** (2023) 1. https://doi.org/10.1186/s40494-022-00833-z
9 T. Li, B. Zhang, W. Xiao, X. Cheng, Z. Li, and J. Zhao: IEEE J. Selected Top. Appl. Earth Obs. Remote Sens. **13** (2023) 4188. https://doi.org/10.1109/JSTARS.2020.3010069
10 S. Lee, D. Han, and M. Song: Sens. Mater. **34** (2022) 12. https://doi.org/10.18494/SAM4192
11 S. Erol, E. Özögel, R. Kuçak, and B. Erol: ISPRS Int. J. Geo-Inf. **9** (2020) 9. https://doi.org/10.3390/ijgi9090528
12 J. Šašak, M. Gallay, J. Kaňuk, J. Hofierka, and J. Minár: Remote Sens. **11** (2019) 8. https://doi.org/10.3390/rs11182154

13 C. Wang, X. Xu, L. Yu, H. Li, and J. Yap: Earth Sci, Inf. **14** (2023) 2. https://doi.org/10.1007/s12145-021-00602-9
14 X. Zhang, P. Zhao, Q. Hu, M. Ai, D. Hu, and J. Li: ISPRS J. Photogramm. and Remote Sens. **159** (2020) 198. https://doi.org/10.1016/j.isprsjprs.2019.11.016
15 M. Guo, M. Sun, T. Zhou, B. Yan, Y. Zhou, and D. Pan: Sens. Mater. **32** (2020) 11. https://doi.org/10.18494/SAM.2020.3052
16 C. Scott, S. DeLong, and J. Arrowsmith: Geophys. Res. Lett. **47** (2020) 22. https://doi.org/10.1029/2020GL090628
17 M. Guo, M. Sun, D. Pan, M. Huang, B. Yan, Y. Zhou, P. Nie, T. Zhou, and Y. Zhao: Measurement **172** (2021) 108765. https://doi.org/10.1016/j.measurement.2020.108765
18 Y. Zhao, B. Sun, S. Liu, C. Zhang, X. He, D. Xu, and W. Tang: ISPRS J. Photogramm. Remote Sens. **180** (2021). https://doi.org/10.1016/j.isprsjprs.2021.08.005
19 J. Li, X. Zhang, and X. Liu: Sens. Mater. **32** (2020) 12. https://doi.org/10.18494/SAM.2020.3136
20 M. Guo, X. Tang, Y. Liu, C. Wang, and Y. Wei: Optics Precis. Eng. **31** (2023) 13.
21 Y. Minkyo, K. Junkyeong, P. Sehwan, L. Taeyoung, and J. Myeong-Hun: Sens. Mater. **32** (2020) 12. https://doi.org/10.18494/SAM.2020.3082
22 X. Liu, J. Ma, and S. Su: Sens. Mater. **32** (2020) 12. https://doi.org/10.18494/SAM.2020.3151